Polat *et al. Earth, Planets and Space* (2016) 68:132
DOI 10.1186/s40623-016-0503-4

Earth, Planets and Space

FULL PAPER Open Access

Investigating P- and S-wave velocity structure beneath the Marmara region (Turkey) and the surrounding area from local earthquake tomography

Gulten Polat[1*], Nurcan Meral Özel[1] and Ivan Koulakov[2,3]

Abstract

We investigated the crustal structure beneath the Marmara region and the surrounding area in the western part of the North Anatolian fault zone. These areas have high seismicity and are of critical significance to earthquake hazards. The study was based on travel-time tomography using local moderate and micro-earthquakes occurring in the study area recorded by the Multi-Disciplinary Earthquake Research in High Risk Regions of Turkey project and Kandilli Observatory and Earthquake Research Institute. We selected 2131 earthquakes and a total of 92,858 arrival times, consisting of 50,044 P-wave and 42,814 S-wave arrival times. We present detailed crustal structure down to 50 km depth beneath the Marmara region for P- and S-wave velocities using the LOTOS code based on iterative inversion. We used the distributions of the resulting seismic parameters (*Vp*, *Vs*) to pick out significant geodynamical features. The high-velocity anomalies correlate well with fracturing segments of the North Anatolian fault. High seismicity is mostly concentrated in these segments. In particular, low velocities were observed beneath the central Marmara Sea at 5 km depth.

Keywords: Marmara Sea, North Anatolian fault zone, Seismic tomography, Seismic velocity structure, Seismicity

Introduction

The Eurasian and Arabian–African plates apply a continuing compressional force on the Anatolian plate (Sengor and Yilmaz 1981). As a result of these intense compressional forces on the Anatolian plate, the northeast–southwest trending North Anatolian fault (NAF) and East Anatolian fault (EAF) were developed (see Fig. 1a). The Anatolian plate in eastern Turkey is moving westward relative to the Eurasia at approximately 40 mm/year (Le Pichon et al. 1995), but begins moving in a southwesterly direction in western Turkey (Jackson 1994). Interaction of this motion and the subduction of the Mediterranean lithosphere beneath the Turkish plate cause a N–S extension and E–W shortening in western Turkey. As a result of this, the region is under extension in a NNE–SSW direction. We focus on the Marmara region, which is one of the most tectonically active regions in the world. Throughout history, many devastating earthquakes (Ambraseys and Zatopek 1969; Karabulut et al. 2003) such as the August 17, 1999 Kocaeli Earthquake (Mw = 7.4) and November 12, 1999 Duzce Earthquake (Mw = 7.2) have occurred in this area. In addition to the devastating earthquakes, typical swarm-type earthquake activity in the Marmara Sea region has also been observed (Ucer et al. 1985; Sellami et al. 1997). Most of the devastating earthquakes are associated with the NAF (Fig. 1a). The NAF poses an important hazard for the large cities surrounding the Marmara Sea region, particularly the megalopolis of Istanbul. Indeed, the NAF is presently hosting a long unruptured segment below the Sea of Marmara (Schmittbuhl et al. 2015). The Marmara Sea is located in a transition zone where the right-lateral strike-slip character of the NAF meets with the extensional character of Aegean (e.g., Smith et al. 1995). In the eastern Sea of Marmara, a transition occurs from

*Correspondence: gultenpolat2005@gmail.com
[1] Department of Geophysics, Kandilli Observatory and Earthquake Research Institute, Boğaziçi University, Istanbul, Turkey
Full list of author information is available at the end of the article

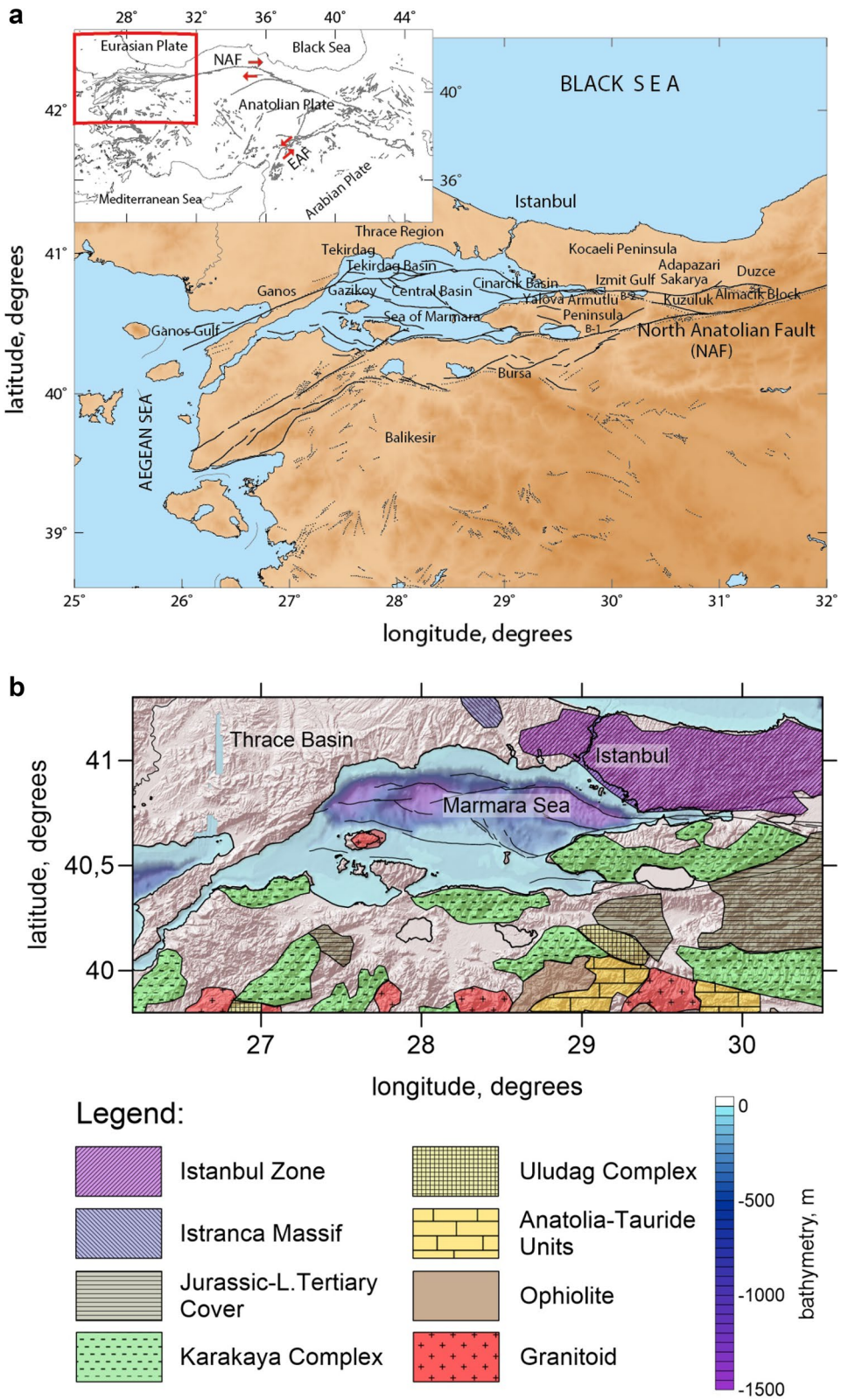

Fig. 1 **a** Tectonic map of Marmara region (*dotted black lines*—faults from Saroglu et al. 1987; *solid black lines*—faults from Armijo et al. 1999). *Inset* location of study area within Turkey is marked within the *red border*. **b** Geological units of the Marmara region modified from Ketin (1967) and Okay (1989)

the right-lateral strike-slip to the Aegean extension zone (Armijo et al. 2005).

Looking at the geologic structure of the study area, the main geologic features of the Marmara region shown in Fig. 1b are primarily composed of three parts, the Sakarya zone (ophiolites, granitoids, and the Karakaya Complex are grouped as Sakarya zone in Fig. 1b), Istanbul zone, and Istranca massif (Ketin 1973; Okay 1989). The Istanbul zone is a small continental fragment, about 400 km long and 70 km wide, located in the southwestern margin of the Black Sea (Fig. 1b). The Istanbul zone is defined by a well-developed, unmetamorphosed, and little deformed continuous Paleozoic sedimentary succession extends from Ordovician to the Carboniferous overlain with a major unconformity by latest Permian to lowermost Triassic continental red beds (Okay 1989). The Istanbul zone is very distinctive from the neighboring tectonic units in its stratigraphy, absence of metamorphism, and lack of major deformation (Okay 1989).

The Sakarya zone is characterized by a variably metamorphosed and strongly deformed Triassic basement called the Karakaya Complex (Fig. 1b) overlain with a major unconformity by Liassic conglomerates and sandstones which passes up to Middle Jurassic-Lower Cretaceous limestones and Upper Cretaceous flysch (Okay 1989). In contrast to the Istanbul zone, the Sakarya zone does not have a Paleozoic basement.

The Izmit Gulf is an east–west trending active graben system that is dynamically affected by the interaction of the NAF and the Marmara Graben system (Onder Cetin et al. 2004). The graben is bounded by two horsts: the Kocaeli Peninsula to the north and the Armutlu Peninsula to the south, showing completely different geomorphological features, and by well-defined fault scarps (e.g., Onder Cetin et al. 2004) (see Fig. 1a, b). The Armutlu Peninsula and the surrounding regions within northwest Anatolia comprise three geologically different zones: southern, central, and northern. The southern zone corresponds to the Sakarya Continent and essentially consists of thick Mesozoic sedimentary successions (Yılmaz et al. 1995**).** The center zone mainly consists of the Iznik metamorphic assemblage and Geyve meta-ophiolite. The northern zone is known as the Armutlu metamorphic assemblage and essentially consists of slightly metamorphosed rocks, interpreted as the Rhodope-Pontide basement (Yılmaz et al. 1995).

In addition to the numerous geological studies mentioned above, many geophysical studies (Okay et al. 2000; Honkura et al. 2000; Baris et al. 2005; Koulakov et al. 2010) have also been done to understand the tectonic evolution and geologic structure of the Marmara region. For example, Baris et al. (2005) applied a 3D local earthquake tomography method to travel time data collected between 1985 and 2002. Strong lateral heterogeneity was observed in the eastern Marmara region. Another important study for this area was conducted by Koulakov et al. (2010). They observed low velocities beneath the main sedimentary basins (e.g., Adapazarı, Düzce, and Kuzuluk shown in Fig. 1a). In the study, high-velocity and low attenuation patterns also correlated with blocks presumed to be rigid (Kocaeli, Armutlu, and Almacik blocks shown in Fig. 1a, b). Furthermore, joint analysis of magnetic and gravity fields, electrical and magnetotelluric measurements (Honkura et al. 1985; Honkura and Isikara 1991; Honkura et al. 2000) has revealed clear anomalous zones related to the variability of the extent of fracturing in different segments of the NAF. Similar features were also found by the analysis of the results of the combined modeling of gravity and reflection seismic data collected in the Marmara Sea region (Adatepe et al. 2002). The crustal seismic structure in the western part of the NAF was investigated by different research groups (e.g., Gurbuz et al. 2000; Nakamura et al. 2002; Baris et al. 2005; Salah et al. 2007) using several tomographic studies. Another study (Karabulut et al. 2003) used a 2D tomographic seismic velocity image in the eastern Marmara region along a N–S trending seismic refraction profile that traverses the Cinarcık Basin in the Sea of Marmara (see Fig. 1a). Most of these studies were based on the inversion of P- and S-wave travel time arrivals from local seismicity recorded by stations belonging to temporary and/or permanent networks. Another important project is a multi-channel marine seismic and 2D wide angle reflection–refraction survey conducted by Laigle et al. (2008) and Bécel et al. (2009), respectively. The projects' profiles give information about depth variations in the basement of up to 7 km between the North Marmara Trough (NMT) and its surroundings. Bayrakci et al. (2013) used the 16,000 first arrival times of artificial sources and inverted them using the well-known local earthquake tomography (LET) code Simulps (Thurber 1983, 1993) to find out the 3D upper-crustal heterogeneity of the NMT. Although these studies cover a similar area, their results often show considerable discrepancies. Polat et al. (2012) investigated crustal anisotropy using shear wave splitting method for the whole Marmara region in detail. They found that decreases in delay times before the impending event, especially at station GEMT, are consistent with the anisotropic poroelasticity (APE) model of fluid-rock deformation. However, similar changes in delay times at other stations surrounding the main event were not observed. Also, this study indicated that the logarithms of the duration of the stress accumulation are proportional (self-similar) to the magnitude of the impending event.

As mentioned above, many studies to understand the region have been conducted, but the detailed crustal structures of the southern part and lower crust of the whole Marmara region have not been obtained. In our study, we aimed to construct a new crustal model of the whole Marmara region using new robust datasets. Considering destructive earthquakes (the August 17, 1999, Mw = 7.4 Kocaeli earthquake and November 12, 1999, Mw = 7.2 Duzce earthquake) in the study area, it can be seen that historical and recent seismicity in the Marmara region is high. This high rate of seismicity has a critical importance for the earthquake hazard in the Marmara region because approximately one-fourth of Turkey's population and most of its industrial centers are located in this region. Therefore, such a study is necessary to obtain robust and reliable information about the detailed crustal structure of the area.

Data and algorithms

In this study, we used broadband and short-period stations (Fig. 2a) installed by Boğazici University, Geophysics Department, Kandilli Observatory and Earthquake Research Institute (KOERI), and the Scientific and Technological Research Council of Turkey (TUBITAK) during the Multi-Disciplinary Earthquake Research in High Risk Regions of Turkey project (TURDEP) in the Marmara Sea region. The short-period and broadband seismic stations must have three components. Additionally, five OBSs (ocean-bottom seismometers) were used (Fig. 2a). All stations from KOERI acquired continuous data between 2005 and 2011. We used the online broadband stations of the TURDEP project. A few stations of the Prime Ministry Disaster and Emergency Management Authority, Republic of Turkey (AFAD) were also used in this work. Most of the used stations are permanent. The OBSs from KOERI recorded earthquakes between 2006 and 2011. During this study, we also added some permanent KOERI stations (Fig. 2b) to our main stations (Fig. 2a) to improve data quality and ray coverage locally. Some of the stations were deployed in this area between 38°–39°N and 26°–30°E. Others were installed in this region between 39°–41°N and 32°–33°E.

For seismic tomography, we relocated approximately 4000 earthquakes with magnitudes ML > 2 occurring from 2005 to 2011 in our study area between the geographical coordinates of 39°–42°N and 25.6°–32°E using zSacWin (Yılmazer 2003). This earthquake processing software is based on HYPO71 (Lee and Lahr 1975). During the relocation procedure of the events, the quality of the recorded three-component waveforms was visually checked. More than 800 events were discarded from the dataset because of poor quality. We paid particular attention to acquiring good signal-to-noise ratio of the incoming wave and to clearly identifying P and S phases on the seismograms. Additionally, we applied a Butterworth filter with a 2–16 Hz band range using a two-way 4-pole on the seismograms in order to suppress the high-frequency noise and correctly determine P and S phases for each seismogram. As mentioned above, arrival times for P and S phases were strictly controlled by visual inspection. Their phases were manually picked with clear P- and S-wave arrivals.

Because of the high attenuation in this region (Horasan et al. 1998; Bindi et al. 2006), noisy and highly attenuated S-wave recordings were observed. To eliminate such recordings, waveforms were carefully examined visually. We thus selected the best possible recordings for further analysis. For relocations, P- and S-wave readings were used, and the magnitudes were always calculated by applying the duration-dependent formula, which is widely used for local earthquakes at KOERI. The duration-dependent formula is useful for small and local earthquakes (Baris et al. 2005). Values of 1.0 and 0.5 were selected as weights for P and S phases for relocations. When relocating events, the P-wave velocity model is used as an initial model. For this, we assumed $Vp/Vs = 1.735$ as generally used by KOERI for routine locations of local seismic events in the western part of Turkey.

Before starting relocation, we noticed that the average horizontal and vertical uncertainties of the collected events were more than 4 and 5 km, respectively. Therefore, we carefully worked to reduce these uncertainties. Further, we constrained the dataset using the criteria that: (1) The standard error of epicenter and depth was less than or equal to 2 km, (2) the number of P phase readings was greater than 7, and (3) the rms of arrival time residuals was less than 0.9 s. In addition, we selected earthquakes with azimuthal gap less than 180° that were recorded by at least seven stations.

The magnitude of the event catalog consists of local moderate and micro-earthquakes with magnitudes ML > 2. Generally, small earthquakes are associated with the NAF segmentation in the Sea of Marmara, whereas the earthquakes with magnitude Mb $\geq$ 5.0 are along the NAF in the Marmara region (Fig. 2b). As observed in Fig. 2b, the observed seismicity in the Sea of Marmara is quite compatible with the known fault geometry (Armijo et al. 2002) located in the sea. However, similar compatibility between earthquakes and the Central and Cınarcık basins was not observed. In particular, the seismicity of the study area intensifies on the left and right boundaries of the northern branch of the NAF in the Sea of Marmara.

Polat et al. (2012) suggested that strong earthquake clusters in the Marmara region before the 2006 Manyas

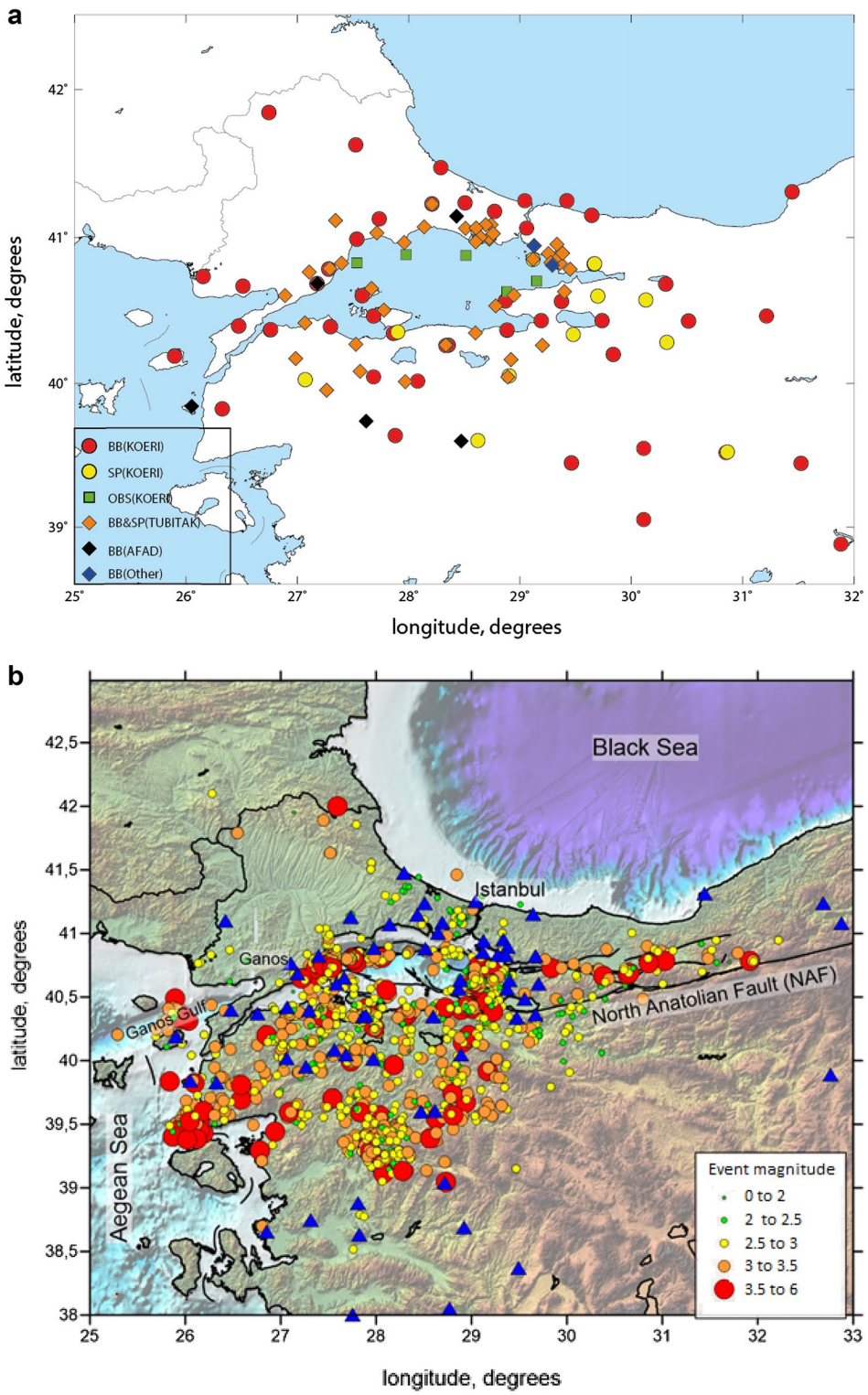

Fig. 2 **a** Seismic station distribution in the study. Broadband (BB) and short-period (SP) stations of KOERI are indicated by *red* and *yellow circles*, respectively. OBS stations of KOERI are shown as *green squares*, and BB and SP stations of TUBITAK are shown as *orange diamonds*. BB stations of the Prime Ministry of Disaster and Emergency Management Authority, Republic of Turkey (AFAD) and BB stations of other institutions are shown as *black* and *light blue diamonds*, respectively. **b** Distributions of seismic stations (*triangles*) and events (*circles*) used in this study. The *colors* of the earthquake symbols indicate the magnitudes

EQ were located in active fault systems in the region (see Fig. 1 in Polat et al. 2012). The 2006 Manyas EQ is the largest event with magnitude Mb = 5.3 within the catalog. After the occurrence of this earthquake, no event greater than magnitude 5.0 has been registered in the Sea of Marmara during the 5-year period of the study. Note that in the southern part of the study area, some events were artificial blasts related to mining work. However, we cannot use them as active sources because their origin times and coordinates are not available from the catalog. Therefore, in our workflow, we process them as passive sources in the same way as earthquakes.

For the tomographic inversion, we selected 2131 events according to two criteria: (1) The number of phase readings of both P and S data is more than 15 in total, and (2) the deviation of residuals after the 1D velocity inversion step is less than 1 s. We thus obtained 50,044 P and 42,814 S travel time data. The selected events are shown in Fig. 2b.

In this study, a local earthquake tomography (LET) method was applied to the selected earthquake data. For the tomographic inversion procedure, we used the LOTOS code (Koulakov 2009). The procedure starts with the relocation of all events using the grid search method. Travel times at this stage were computed using a reference table calculated prior to the relocation step. The sources were relocated using the 3D algorithm of ray tracing. The first iteration used a starting 1D model, but in the next iterations, the relocation was performed using the updated 3D velocity models. The ray tracing was performed using the bending method.

The starting 1D velocity model was defined at several depth levels with linear interpolation between levels. The upper level of the 1D model was defined at the altitude above the maximum elevation in the study region. The optimal 1D starting model for the 3D tomography inversion was determined after several runs of the full inversion procedure, including inversions and source locations in several iterations. We begin with an approximate 1D model constrained from available a priori information. After full inversion, we computed average absolute velocities at several depth levels and used these values as a starting 1D model for the next run. After three or four runs, the velocities converged to stable values and the procedure stopped. Table 1 presents the resulting P and S velocities used as a reference model for the main results. Note that at shallower depths, we observe higher velocities than usually expected in continental areas.

The parameterization of the velocity distribution was performed using a mesh of nodes distributed in the study area according to the data distribution. In this study, the minimum grid spacing was 7 km in horizontal direction and 3 km in the vertical. In our case, we used

Table 1 P- and S-wave velocities in the 1D model used for calculations of the main results of this study

Depth (km)	*Vp* (km/s)	*Vs* (km/s)
−1	5.63	3.19
5	6.03	3.46
10	6.21	3.53
15	6.36	3.62
20	6.61	3.77
30	7.31	4.21
40	7.76	4.46
50	7.97	4.52
100	8.3	4.75

~18,000 and ~16,000 nodes, which composed one grid for the P and one grid for the S model, respectively. The grid spacing was explicitly defined to be smaller than the minimum size of resolved anomalies so that every robust pattern in the resulting model included several nodes. In this case, the solution becomes grid independent: Changing the mesh (i.e., shifting or rotating the grid) does not affect the solution. However, to further minimize artefacts related to the basic grid orientation, we performed independent inversions for four grids with different basic orientations (0°, 22°, 45°, and 67°).

The inversion was performed simultaneously for the P- and S-velocity anomalies, as well as for the source parameters (three coordinates and origin time for each event) and station corrections. The quality of the solution was controlled by additional matrix blocks, which regularize velocity gradients between neighboring nodes. This regularization links the velocity parameters in all pairs of neighboring nodes and makes the parameterization quasi-continuous. In this case, the resolution was controlled by the flattening coefficients, and not by properties of the grid. The values of damping parameters and weights for different groups of parameters were defined experimentally based on results of different tests. In particular, the correct smoothing coefficient should not allow for appearance of small contrasted patterns, which cannot be resolved by synthetic tests and are not similarly observed in the odd/even test.

The sparse matrix was inverted using the least-squares QR method (Paige and Saunders 1982; van der Sluis and van der Vorst 1987). After inversions in four differently oriented grids, the results were averaged and recomputed in a regular grid. This model was used as a reference distribution for the next iteration, which starts with the relocation of sources. The tomography cycle, which was repeated several times, included the steps of source locations in the updated 3D model, matrix calculation, and inversion. The effect of iterating and damping was

similar: Many iterations with strong damping result in a solution similar to that from few iterations and weak damping. Therefore, we preferred to fix the number of iterations at five, as a compromise between the accuracy and calculation speed, and selecting damping coefficients to find an appropriate solution.

After five iterations, the rms values of the P and S arrival time residuals and their reductions were obtained. They are presented in Table 2. The residuals of the first iteration correspond to the location in the constructed 1D model. Other iteration values in Table 2 indicate how the 3D velocity inversion leads to an improved data fit. The values of the residuals obtained from the dataset are quite different initially (0.238 and 0.419 s for P and S data, respectively) compared to those for a dataset collected in the eastern Marmara region. For example, for the eastern Marmara region (Koulakov et al. 2010), in the first iteration, the rms of P and S residuals was 0.137 and 0.255 s, respectively. It is significant that the same algorithm was used for data processing both in the present and in the mentioned study. This might suggest that for an a priori indicator of the amplitude of the velocity anomalies, it is possible to use the rms of the initial residuals.

The average deviations of residuals in the L1 norm during iterative inversions are presented in Table 2. It can be seen that the inversion provides the reduction in residual deviations by approximately 30 % for P- and 47.5 % for S-wave data. The final average deviations are consistent with estimates of the picking accuracy (0.15 and 0.20 s for P and S phases, respectively). Larger reduction of residuals for the S data might be related to higher sensitivity of the S data to variations in physical parameters inside the Earth.

Tomography results and testing

P- and S-velocity anomalies in four horizontal slices at 5, 15, 30, and 50 km depth are shown in Fig. 3. The P- and S-velocity anomalies are also depicted for one vertical section in Fig. 4. At shallow depths, their amplitudes were less than 5 %, whereas at a depth of 30 km, they were less than 2 %. In the inversion, we removed the amplitude damping and defined the smoothing damping at a minimal value, providing stable results. The values of the inversion parameters were set according to the results of synthetic modeling, enabling maximum similarity between the initial and recovered models, both in terms of amplitude and the positions of the synthetic patterns.

Table 2 Average deviations in the L1 norm of the P- and S-wave residuals and variance reductions after five inversion iterations

Iteration	rms dtp[a] (s)	rms dts[a] (s)	Reduction P (%)	Reduction S (%)
1	0.238	0.419	0	0
2	0.183	0.250	22.84	40.41
3	0.172	0.230	27.50	45.18
4	0.167	0.222	29.57	46.89
5	0.166	0.220	30.20	47.46

[a] rms dtp and rms dts stand for P- and S-wave residuals, respectively

Before interpreting these results, we present a few tests to assess the resolution and the reliability of the derived structures. In Fig. 5, we present the results of several checkerboard tests. Here, we show the reconstruction results for the models with anomaly sizes of 20, 30, and 50 km and amplitudes of ±5 %. Travel times for the synthetic tests were computed using the 3D bending ray tracing based on the same source—receiver pairs as in the actual dataset. Then, they were perturbed by random noise with an rms of 0.1 s for P- and S-wave data, respectively. The reconstruction workflow and parameters were absolutely identical to those implemented for the analysis of experimental data, including the step of the initial source location. In Fig. 5, we show only results for the P-velocity reconstructions; for the S model, the reconstruction quality was similar and even better. It can be seen that at shallow depths (left column), all models are correctly reconstructed in most parts of the area. The sections in the right column represent the deepest sections where the satisfactory recovery of synthetic anomalies is achieved. It can be seen that the anomalies of 20 km size are robustly reconstructed down to 15 km depth; 30 km anomalies are seen down to 30 km depth, whereas the 50 km anomalies are restored in all depth intervals. From these tests, we can conclude that the ray configuration theoretically allows for reconstructing the shapes of small patterns at shallow depths only, whereas the large anomalies of more than 50 km size are robustly recovered at all depths. Note, however, that the amplitude of the reconstructed anomalies decays with depth. These observations should be taken into account when interpreting the results of experimental data inversion.

A much more important test with independent inversions of two independent data subsets, the so-called odd/even test, is presented in Fig. 6. In this case, the entire dataset is divided into two subsets with odd and even numbers of events. The difference between the derived results reflects the effect of random noise. For the P-model, the locations of the main anomalies are similar in both cases; however, their shapes and amplitudes in some parts of the study area are different. For the S-wave velocity anomalies, the relatively robust features are resolved at shallow depths. For the deeper section,

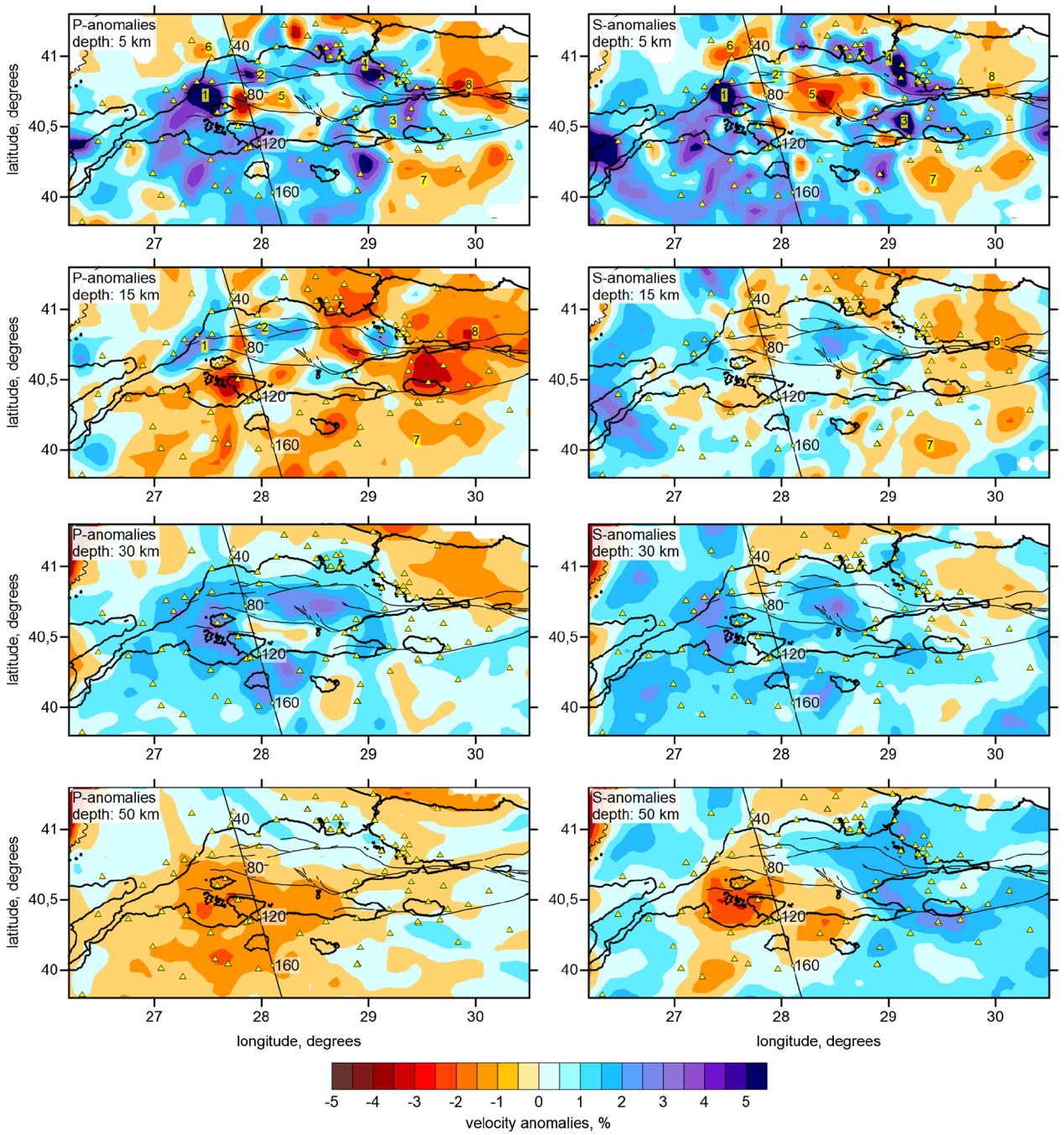

Fig. 3 P- and S-velocity anomalies in *four horizontal sections*. *Triangles* depict seismic stations. Major faults in the Marmara Sea (same as in Fig. 1a) are depicted with *thin lines*. *Black line* shows one *vertical section* selected for depicting the P- and S-velocity anomalies in Fig. 4

the anomalies derived from the odd and even subsets do not match, indicating the important role of the random factor. Thus, the corresponding results should be interpreted with prudence.

Discussion

The resulting distributions of seismic velocities obtained from this study indicate clear correlation with the known tectonic features of the study area. P- and S-wave velocity anomalies are shown in Fig. 3 in four horizontal slices

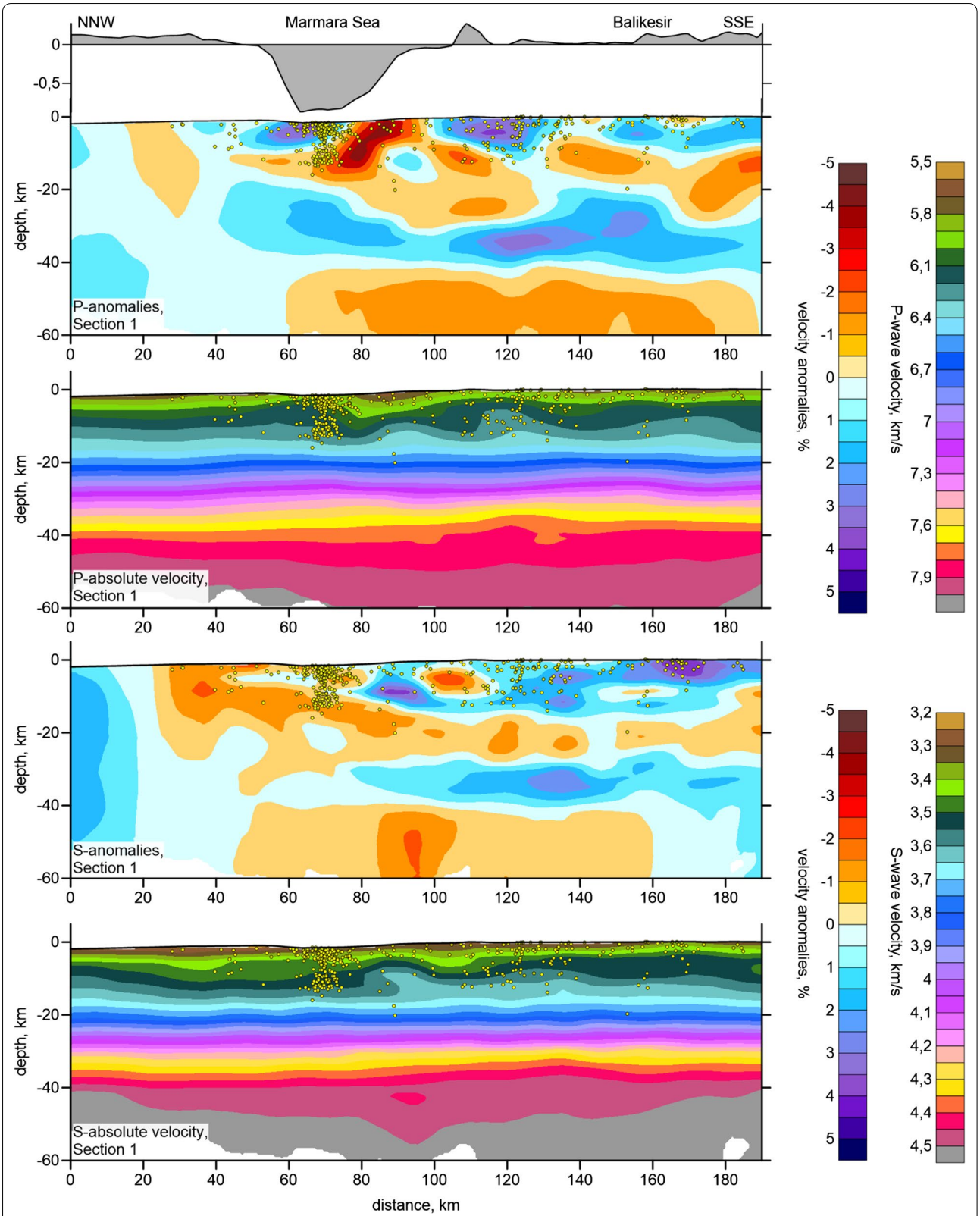

Fig. 4 Perturbations and absolute values of P- and S-wave velocities in a *vertical section*. Location of the profile is shown in Fig. 3. *Dots* represent the seismic events located at distances less than 15 km from the profile. The topography along the profile is shown in the *upper part* of the figure. Note that the upper surface in the velocity sections takes into account the earth's sphericity

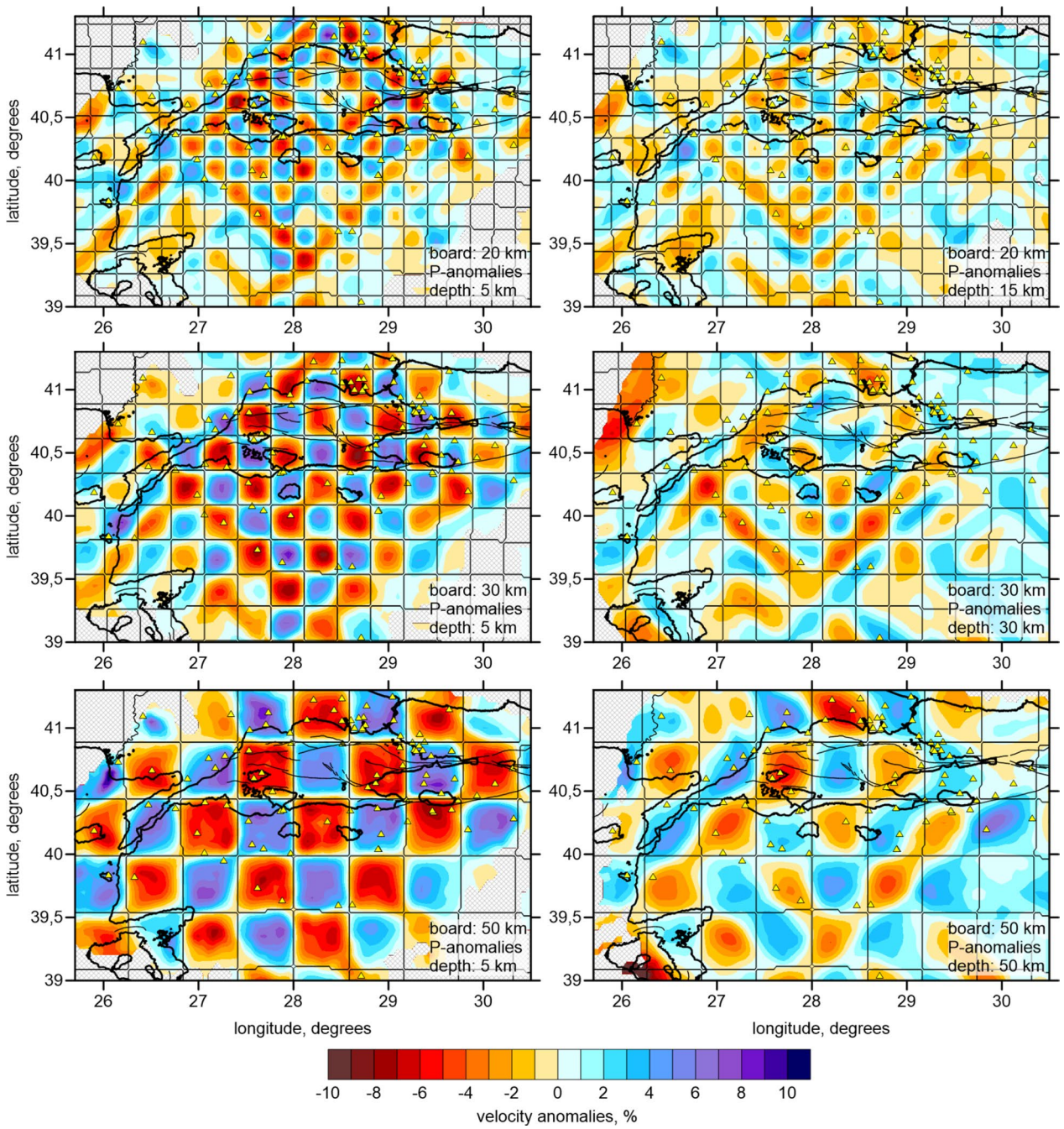

Fig. 5 Reconstructions of three checkerboard tests with anomaly spacing of 20, 30, and 50 km. The *shallower section* is at 5 km depth, and the *deeper sections* are at different depths corresponding to the deepest level where the recovery is satisfactory. *Shapes* of *anomalies* are indicated with *thin line* contours. *Triangles* depict seismic stations

at 5, 15, 30, and 50 km depths and in one vertical section (Fig. 4).

We see that in most parts of the model, the P and S anomalies are generally similar. Some differences in detail can be explained by the complex structure of the crust in this region. In our case, in the Marmara Sea region, the crust has a complex structure with strongly varied composition and fracture zones strongly saturated with fluids. For example, relict igneous bodies will be mostly associated with higher P-velocities, as this parameter is mostly

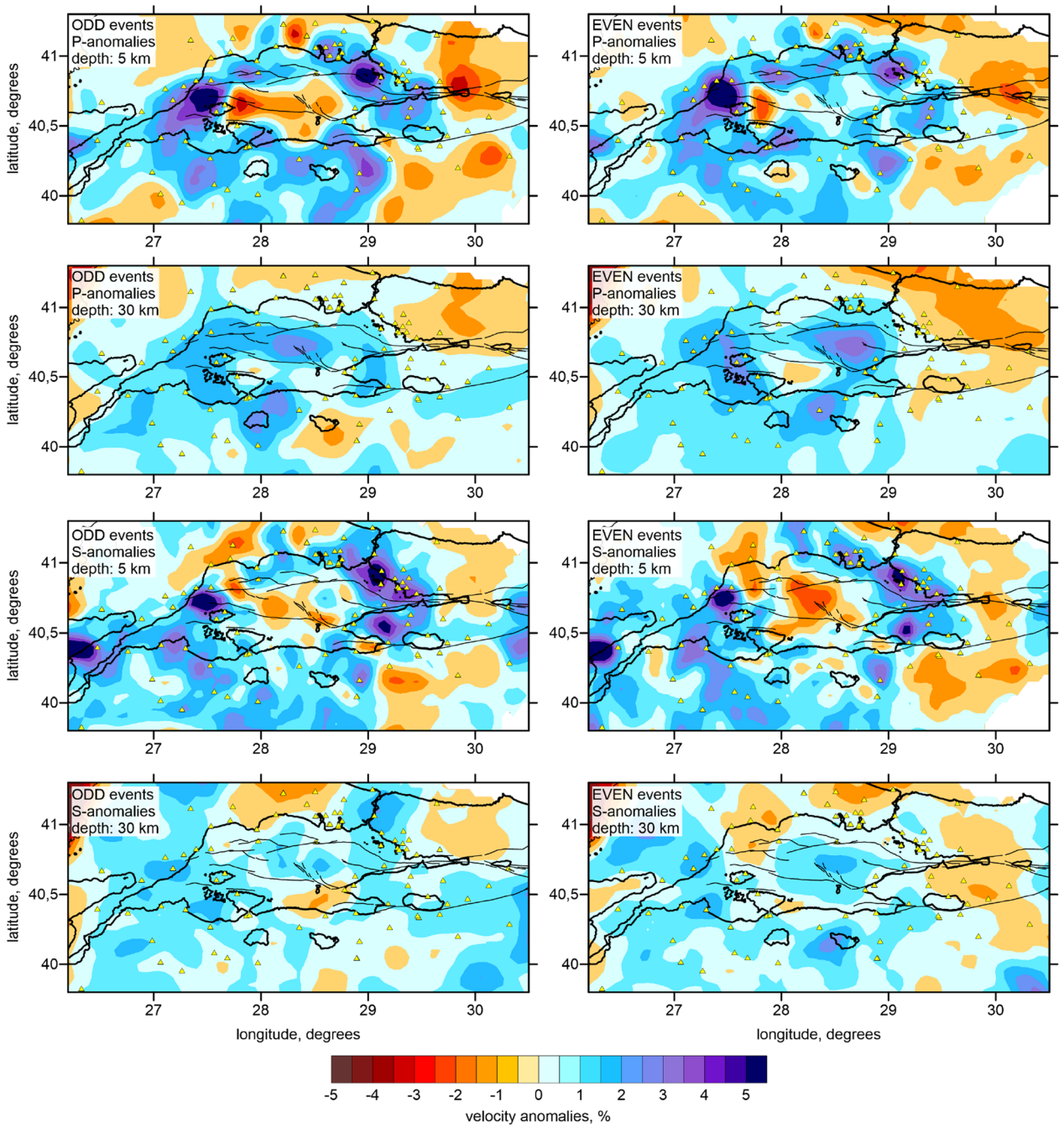

Fig. 6 Odd/even test. *Left* and *right columns* are reconstruction results for independent data subsets with odd and even numbers of events, respectively. *Triangles* depict seismic stations. Major faults in the Marmara Sea (same as in Fig. 1a), are depicted with thin *lines*

sensitive to the composition. However, if these rocks were fractured and saturated with liquid fluids, S-wave velocity would be drastically lowered. The opposite correlation of the P and S anomalies is often observed in volcanic areas and usually associated with active magma conduits with partially molten rocks (e.g., Koulakov et al. 2013, 2015). In areas of active faults, the relationships between P and S anomalies are mostly controlled by the presence of igneous rocks and the degree of fracturing and saturation with liquid or gas fluids. These and many other factors may affect the P- and S-velocity differently and lead to some misfit of the P and S anomalies.

The shallow part of the crust beneath the Marmara Sea shows significant lateral velocity variations. The striking feature of this study is that, besides a low-velocity anomaly in the central part of the Marmara Sea, there are several high-velocity anomalies located onshore at a depth of 5 km. At this depth interval, relative high P- and S-velocity values at shallow depths are found in Yalova, Gazikoy, and Tekirdag (Anomalies 1 and 2 in Fig. 3). This observation is consistent with high seismic activity in these areas and the findings of Koulakov et al. (2010). Additionally, high-velocity values are located underneath the Sakarya Zone and the Armutlu Peninsula (Anomaly 3 in Fig. 3). The Armutlu Peninsula is dominated by metamorphic assemblages (Yılmaz et al. 1995). Other observed high velocities are located beneath the Istanbul zone (Anomaly 4 in Fig. 3), corresponding to a well-developed, unmetamorphosed, and little deformed continuous Paleozoic sedimentary succession extends from Ordovician to Carboniferous (Ketin 1973).

In contrast, we observed low-velocity values beneath the central Marmara Sea region (Anomaly 5 in Fig. 3), which is seen especially well in the S-wave velocity model at shallow depths. We suggest that it might correspond to the thick sedimentary deposits of the Plio-Pleistocene or to the alluvium regions as supported by the low resistivity and gravity values (Kaya et al. 2013; Bayrakci et al. 2013).

In the Thrace region, we observe a negative anomaly in the P and S models (Anomaly 6 in Fig. 3), which seem consistent with the known geologic composition of the area that is composed of the Late Tertiary deposit basin. In the southern part of the Tekirdag Basin, low-velocity values are detected at a depth of 15 km. The observed low-velocity anomalies are not consistent with active seismicity in the basin and its vicinity. Geological studies (e.g., Okay et al. 1999) indicate that this basin was formed in the Pliocene. Because of its relatively young age, the sediments in the basin are not strongly deformed, which suggests a subtle relationship between the faulting and sedimentation. Similar features can be seen in many strike-slip basins, and they often introduce an element of ambiguity into the tectonic setting of these basins (Ingersoll and Busby 1995). Armijo et al. (2005) showed that the Tekirdag Basin region had a NW–SE trending transtensional state with almost purely normal fault mechanisms with some right-lateral strike-slip and a few oblique components. Additionally, low P and S anomalies (Anomaly 7) are observed in the southern Marmara region, particularly Balikesir and Bursa, and the surrounding areas at 5 and 15 km depths. At these depths, areas with high P-wave velocities are significantly reduced. Additionally, at these depths, we observed that low-velocity areas are gradually extended. The observed anomalies seem remarkably consistent with the known geologic features and tectonic evolution of the region and the surrounding area. Recently, in the interior of the southern Marmara region, one of the studies conducted by Erkan (2015) shows moderate heat-flow values. As known, the heat flow remarkably influences seismic velocities. This finding seems compatible with and explains the low-velocity anomaly (Anomaly 7).

Moreover, at 5 km depth, high P- and S-wave velocity variations are observed in the Kuzuluk Basin and surrounding areas. However, similar patterns in this area are not observed at 15 km depth. The focal mechanism study of Tibi et al. (2001) found west–east extension in the Kuzuluk Basin. Also, many thermal sources (e.g., Greber 1994; Belin et al. 2002) support the concept of an active pull-apart extension. A similar mechanism of pull-apart basin opening was earlier proposed for the Marmara Sea (e.g., Armijo et al. 1999; Pondard et al. 2007). In the context of the findings, it can be said that the low-velocity anomalies observed at 15 km depth in this region might be related to the pull-apart basin. At 5 and 15 km depths, low-velocity anomalies (Anomaly 8 in Fig. 3) are observed beneath the small region between the eastern region of the Izmit Gulf and the Kuzuluk Basin. This suggests that it is possible to extend the anomaly area up to the sedimentary basins (e.g., Adapazarı, Düzce). In this case, no suggestions can be made about the Almacik block because of the unavailability of data.

The region between the two branches (the branches denoted B-1 and B-2 in Fig. 1a) of the NAF is expressed by relatively high seismicity (the cluster of events mainly located in the segments shown in Fig. 2b). Looking at the distribution of low and high-velocity anomalies in the region, we see that a large low-velocity pattern is observed beneath the center of the region, even though relatively high-velocity anomalies are observed near the segments. This suggests that the observed high-velocity zones correspond to high resistivity zones (e.g., Tank et al. 2005). According to the study of Tank et al. (2005), these high resistivity zones correspond to an asperity that is characterized by strong coupling at the fault interface. A similar asperity zone is pointed out by Delouis et al. (2000) around the hypocenter in their joint inversion study of InSAR and teleseismic data.

P-wave velocities within the lower crust beneath the western and southern parts of the Marmara region (e.g., Ganos, Ganos Gulf, Balikesir, Bursa, and the surrounding areas of the places shown in Fig. 1a), below a depth of 30 km, gradually increase. However at 50 km depth, the P-wave velocity decreases strongly (Fig. 3). This may be related to the fact that the east–west trending normal fault systems of the Sea of Marmara are a diffuse zone of crustal thinning associated with an estimated 30 % of north–south extension since the Tortonian (Ergün et al. 1995). Also, we observed that the resolution for the

S-wave is as good as that for the P-wave. Therefore, we can discuss the structure of *V*p and *V*s in the crust of the Marmara region. Although below 15 km depth the resolution is poor because of insufficient earthquake data, at 50 km depth, for both the P- and S-velocity models, we identify a low-velocity anomaly beneath the western part of the Marmara Sea, which can be interpreted as an asthenosphere upwelling. In turn, such upwelling might cause thermal weakening of the crust that initiated the process of crustal extension in the area of the Marmara Sea.

Conclusion

In this study, we collected data from permanent and temporary stations deployed by TUBITAK during the TURDEP and KOERI in order to investigate the P- and S-wave velocity structure beneath the whole Marmara region and western Turkey. For this study, local earthquakes from 2005 to 2011 were analyzed. After relocation of the events, we derived 2131 earthquakes and a total of 92,858 arrival times, consisting of 50,044 P-wave and 42,814 S-wave arrival times for the LET.

Our observations suggest that the LET has been successfully applied to measure P- and S-wave velocity variations for the whole Marmara region. At the depth interval of 5–15 km, the presence of velocity variations between land and the central Marmara Sea region is clearly observed. At this depth interval, high P- and S-wave velocity values are observed beneath Armutlu Peninsula, Yalova, Gazikoy, and Tekirdağ. High-velocity values in the Sakarya zone are observed. Looking at the distribution of low-velocity anomalies, a large low-velocity pattern is observed beneath the central Marmara Sea region. The observed high-velocity anomalies extend between the two branches of the NAF and might correspond to the high resistivity zone. We observed that the shallow part of the crust beneath the Marmara Sea shows significant lateral velocity variations. The striking feature of this study is that a clear pattern is also observed in between the on-land and the central Marmara Sea region at the depth interval of 5–15 km.

Abbreviations

AFAD: Prime Ministry Disaster and Emergency Management Authority, Republic of Turkey; EAF: East Anatolian fault; KOERI: Boğaziçi University, Geophysics Department, Kandilli Observatory and Earthquake Research Institute; LET: Local earthquake tomography; MARsite: New directions in seismic hazard assessment through focused earth observation in the Marmara supersite; NAF: North Anatolian fault; NMT: North Marmara trough; OBS: Ocean-bottom seismometer; TUBİTAK: Scientific and Technological Research Council of Turkey; TURDEP: Multi-Disciplinary Earthquake Research in High Risk Regions of Turkey Project.

Authors' contributions

NMO significantly contributed to the conception and design of the paper and contributed to the acquisition of data. GP carried out the analysis and interpretation of data and drafted the manuscript, including its intellectual contents. IK applied checkerboard tests and interpreted the results and drafted the manuscript, including its intellectual contents. GP, NMO, and IK are responsible for final approval, accountability, and accuracy. All authors read and approved the final manuscript.

Author details

[1] Department of Geophysics, Kandilli Observatory and Earthquake Research Institute, Boğaziçi University, Istanbul, Turkey. [2] Trofimuk Institute of Petroleum Geology and Geophysics, SB RAS, Prospekt Koptyuga 3, Novosibirsk, Russia 630090. [3] Novosibirsk State University, Pirogova 2, Novosibirsk, Russia 630090.

Acknowledgements

This study was partly supported by EC/FP-7 Project "MARSite: New Directions in Seismic Hazard assessment through Focused Earth Observation in the Marmara Supersite" (Grant Agreement No: 329 308417). This study has benefited from the JICA/SATREPS Project "MarDIM: Earthquake and Tsunami Disaster Mitigation in the Marmara Region and Disaster Education in Turkey". Ivan Koulakov was also supported by the Russian Scientific Foundation (Grant No. 14-17-00430). We are grateful to three anonymous reviewers for rigorous criticism and constructive comments, which helped us to improve the paper. The authors thank Esen Arpat for inspiring discussions on the North Anatolian fault and Marmara region. Finally, the authors would like to thank Carol-Anne Frame from the British Geological Survey for English editing of our manuscript.

Competing interests

The authors declare that they have no competing interests.

Received: 19 October 2015 Accepted: 5 July 2016
Published online: 22 July 2016

References

Adatepe F, Demirel S, Alpar B (2002) Tectonic setting of the southern Marmara Sea region based on seismic reflection data and gravity modelling. Mar Geol 190:383–395

Ambraseys NN, Zatopek A (1969) The Mudurnu Valley earthquake of July 22nd 1967. Bull Seism Soc Am 59:521–589

Armijo R, Meyer B, Hubert A, Barka A (1999) Westward propagation of the North Anatolian fault into the northern Aegean: timing and kinematics. Geology 27:267–270

Armijo R, Meyer B, Navarro S, King G, Barka A (2002) Asymmetric slip partitioning in the Sea of Marmara pull-apart: a clue to propagation processes of the North Anatolian Fault? Terra Nova 14:80–86

Armijo R, Pondard N, Meyer B, Mercier de Lépinay B, Uçarkus G (2005) Submarine fault scarps in the Sea of Marmara pull-apart (North Anatolian Fault): implications for seismic hazard in Istanbul. Geochem Geophys Geosyst. doi:10.1029/2004GC000896

Baris S, Nakajima J, Hasegawa A, Honkura Y, Ito A, Ucer SB (2005) Three-dimensional structure of V_P, V_S, and $V_P = V_S$ in the upper crust of the Marmara region, NW Turkey. Earth Planets Space 57(11):1019–1038

Bayrakci G, Laigle M, Bécel A, Hirn A, Taymaz T, Yolsal-Cevikbilen S, SEISMARMARA team (2013) 3-D sediment-basement tomography of the Northern Marmara trough by a dense OBS network at the nodes of a grid of controlled source profiles along the North Anatolian fault. Geophys J Int 194:1335–1357

Bécel A, Laigle M, de Voogd B, Hirn A, Taymaz T, Galvé A, Shimamura H, Mura Y, Lépine J, Sapin M, Özalaybey S (2009) Moho, crustal architecture and deep deformation under the North Marmara trough, from the Seismarmara leg1 offshore-onshore reflection-refraction survey. Tectonophysics 467:1–21

Belin B, Yalçin T, Suner F, Bozkurtoglu E, Gelir A, Güven H (2002) Earthquake-related chemical and radioactivity changes of thermal water in Kuzuluk-Adapazari, Turkey. J Env Radioact 63(3):239–249

Bindi D, Parolai S, Grosser H, Milkereit C, Karakisa S (2006) Crustal attenuation characteristics in Northwestern Turkey in the range from 1 to 10 Hz. Bull Seismol Soc Am 96(1):200–214

Delouis B, Lundgren P, Salichon J, Giardini D (2000) Joint inversion of InSAR and teleseismic data for the slip history of the 1999 Izmit (Turkey) earthquake. Geophys Res Lett 27(20):3389–3392

Ergün M, Özel E, Sari C (1995) Structure of the Marmara Sea within the North Anatolian Fault zone. In: Banda E, Talwani M, Torne M (eds) NATO ARW book "Ritted ocean-continent boundaries". NATO ASI Series. Kluwer Academic Publishers, Dordrecht, Boston, London, pp 309–326

Erkan K (2015) Geothermal investigations in western Anatolia using equilibrium temperatures from shallow boreholes. Solid Earth 6(1):103–113

Greber E (1994) Deep circulation of CO2-rich paleowaters in deep seismically active zone (Kuzuluk/Adapazarı, northwestern Turkey). Geothermics 23:151–174

Gurbuz C, Aktar M, Eyidoğan H, Cisternas A, Haessler H, Barka A, Ergin M, Türkelli N, Polat O, Üçer SB, Kuleli S, Barış Ş, Kaypak B, Bekler T, Zor E, Biçmen F, Yörük A (2000) The seismotectonics of the Marmara region (Turkey): results from a micro-seismic experiment. Tectonophysics 316:1–17

Honkura Y, Isıkara AM (1991) Multidisciplinary research on fault activity in the western part of the North Anatolian Fault Zone. Tectonophysics 193:347–357

Honkura Y, Isıkara AM, Kolcak D, Orbay N, Sipahioglu S, Ohshiman S, Tanaka H (1985) Magnetic anomalies and low ground resistivity as possible indicators of active fault location: preliminary results of electric and magnetic observations from the western part of the North Anatolian Fault Zone. J Geomag Geoelectr 37:169–187

Honkura Y, Isıkara AM, Oshiman N, Ito A, Ucer B, Baris B, Tuncer MK, Matsushima M, Pektas R, Celik C, Tank SB, Takahashi F, Yoshimura R, Ikeda Y, Komut T (2000) Preliminary results of multidisciplinary observations before, during and after the Kocaeli (Izmit) earthquake in the western part of the North Anatolian Fault Zone. Earth Planets Space 52:293–298

Horasan G, Kaslılar-Ozcan A, Boztepe-Guney A, Turkelli N (1998) S-wave attenuation in the Marmara region, northwestern Turkey. Geophys Res Lett 25(14):2733–2736

Ingersoll RV, Busby CJ (1995) Tectonics of sedimentary basins. In: Busby CJ, Ingersoll RV (eds) Tectonics of sedimentary basins. Blackwell Science, Oxford

Jackson J (1994) Active tectonics of the Aegean region. Annu Rev Earth Planet Sci 22:239–271

Karabulut H, Özalaybey S, Taymaz T, Aktar M, Selvi O, Kocaoğlu A (2003) A Tomographic Image of the Shallow Crustal Structure in the Eastern Marmara. Geophys Res Lett 30(24):2277

Kaya T, Kasaya T, Tank B, Ogawa Y, Tunçer M, Oshiman N, Honkura Y, Matsushima M (2013) Electrical characterization of the North Anatolian Fault Zone underneath the Marmara Sea, Turkey by ocean bottom magnetotellurics. Geophys J Int. doi:10.1093/gji/ggt025

Ketin I (1967) Bolu–Gerede–Mengen ve Yıgılca bolgesindeki Paleozoyik olusuklara ait jeolojik rapor, TPAO Arama Grubu Rap No: 379, unpublished (in Turkish)

Ketin I (1973) Genel Jeoloji (General Geology), Published by İTÜ, 4th Ed

Koulakov I (2009) LOTOS code for local earthquake tomographic inversion. Benchmarks for testing tomographic algorithms. Bull Seismol Soc Am 99(1):194–214. doi:10.1785/0120080013

Koulakov I, Bindi D, Parolai S, Grosser H, Milkereit C (2010) Distribution of seismic velocities and attenuation in the crust beneath the North Anatolian fault (Turkey) from local earthquake tomography. Bull Seism Soc Am 100(1):207–224. doi:10.1785/0120090105

Koulakov I, West M, Izbekov P (2013) Fluid ascent during the 2004–2005 unrest at Mt. Spurr inferred from seismic tomography. Geophys Res Lett 40(17):4579–4582. doi:10.1002/grl.50674

Koulakov I, El Khrepy S, Al-Arifi N, Kuznetsov P, Kasatkina E (2015) Structural cause of a missed eruption in the Harrat Lunayyir basaltic field (Saudi Arabia) in 2009. Geology G36271:1. doi:10.1130/G36271.1

Laigle M, Bécel A, de Voogd B, Hirn A, Taymaz T, Ozalaybey S, Members of SEISMARMARA Leg1 Team (2008) A first deep seismic survey in the sea of Marmara: deep basins and whole trust architecture and evolution. Earth Planet Sci Lett 270:168–179

Le Pichon X, Chamot-Rooke N, Lallemant S (1995) Geodetic determination of the kinematics of central Greece with respect to Europe: implications for eastern Mediterranean tectonics. J Geophys Res 100(12):675–690

Lee WHK, Lahr JC (1975) HYP071 (revised): a computer program for determining hypocenter, magnitude, and first motion pattern of local earthquakes. US Geological Survey Open File Report, vol 113, pp 75–311

Nakamura A, Hasegawa A, Ito A, Ucer SB, Baris S, Honkura Y, Kono T, Hori S, Pektas R, Komut T, Celik C, Isikara AM (2002) P-wave velocity structure of the crust and its relationship to the occurrence of the 1999 Izmit, Turkey earthquake and aftershocks. Bull Seism Soc Am 92:330–338

Okay AI (1989) Tectonic units and sutures in the Pontides, northern Turkey. In: Sengor AMC (ed) Tectonic evolution of the Tethyan region. NATO advanced ASI series. Kluwer Academic Publications, Dordrecht, pp 109–116

Okay AI, Demirbağ E, Kurt H, Okay N, Kusçu I (1999) An active, deep marine strike-slip basin along the North Anatolian fault in Turkey. Tectonics 18:129–148

Okay AI, Kaşlılar-Özcan A, İmren C, Boztepe-Güney A, Demirbağ E, Kuscu I (2000) Active faults and evolving strike-slip basins in the Marmara Sea, northwest Turkey: a multichannel seismic reflection study. Tectonophysics 321:189–218

Onder Cetin K, Isik N, Unutmaz B (2004) Seismically induced landslide at Degirmendere Nose, Izmit Bay during Kocaeli (Izmit)-Turkey earthquake. Soil Dyn Earthq Eng 24:189–197

Paige CC, Saunders MA (1982) LSQR, An algorithm for sparse linear equations and sparse least squares. ACM Trans Math Soft 8:43–71

Polat G, Ozel NM, Crampin S, Ergintav S, Tan O (2012) Shear wave splitting as a proxy for stress forecast of the case of the 2006 Manyas-Kus Golu (Mb = 5.3) earthquake. Nat Hazards Earth Syst Sci 12:1073–1084. doi:10.5194/nhess-12-1073

Pondard N, Armijo R, King GCP, Meyer B, Flerit F (2007) Fault interactions in the Sea of Marmara pull-apart (North Anatolian fault): earthquake clustering and propagating earthquake sequences. Geophys J Int 171:1185–1197

Salah MK, Sahin S, Kaplan M (2007) Seismic velocity structure along the western segment of the North Anatolian fault zone imaged by seismic tomography. Bull Earthq Res Inst Univ Tokyo 82:209–223

Saroglu F, Boray A, Emre O (1987) Active faults of Turkey, dissertation, Mineral Research and Exploration Institute of Turkey

Schmittbuhl J, Karabulut H, Lengline O, Bouchon M (2015) Seismicity distribution and locking depth along the main Marmara Fault, Turkey. Geochem Geophys Geosyst. doi:10.1002/2015GC00612

Sellami S, Pavoni N, Mayer-Rosa D, Mueller St, Eyidogan H, Aktar M, Gürbüz C, Baris S, Polat O, Yalcin N (1997) Seismicity and seismotectonics of the Bursa region. In: Schindler C, Pfister M (eds) Active tectonics of Northwestern Anatolia—the Marmara poly-project, a multidisciplinary approach by Space-Geodesy, Geology, Hydrogeology, Geothermics and Seismology, vdf Zürich, pp 149–185

Sengor AMC, Yilmaz Y (1981) Tethyan evolution of Turkey: a plate tectonic approach. Tectonophysics 75:181–241

Smith A, Oktay F, Taymaz T, Jackson J, Başaran H, Alpar B, Şimşek M, Kara S (1995) High resolution of seismic profiling in the Sea of Marmara-NW Turkey: late Quaternary sedimentation and sea-level changes. GSA Bull 197:923–936

Tank B, Honkura Y, Ogawa Y, Matsushima M, Oshiman N, Tunçer MK, Çelik C, Tolak E, Işıkara AM (2005) Magnetotelluric imaging of the fault rupture area of the 1999 İzmit (Turkey) earthquake. Phys Earth Planet Inter 150(1–3):213–225

Thurber CH (1983) Earthquake locations and three-dimensional crustal structure in the Coyote Lake area, central California. J Geophys Res 88:8226–8236

Thurber CH (1993) In: Iyer HM, Hirahara K (eds) Local earthquake tomography: velocities and Vp/Vs-theory, in Seismic Tomography: theory and practice. Chapman and Hall, London

Tibi R, Bock G, Xia Y, Baumbach M, Grosser H, Milkereit C, Karakisa S, Zübül S, Kind R, Zschau J (2001) Rupture processes of the August 17 İzmit and November 12, 1999, Düzce (Turkey) earthquakes. Geophys J Int 144(2):F1–F7

Ucer SB, Crampin S, Evans R, Miller A, Kafadar N (1985) The MARNET radiolinked seismometer network spanning the Marmara Sea and the seismicity of Western Anatolia. Geophys J R Astr Soc 83:17–30

Van der Sluis A, van der Vorst HA (1987) In: Nolet G (ed) Numerical solution of large, sparse linear algebraic systems arising from tomographic problems, in Seismic Tomography. Reidel, Dortrecht

Yılmaz Y, Genc S C, Yigitbas E, Bozcu M, Yılmaz K (1995) Geological evolution of the late Mesozoic continental margin of the North western Anatolia. Tectonophysics 243:155–171

Yılmazer M (2003) zSacWin (Kandilli earthquake processing software) developed for KOERI. http://www.koeri.boun.edu.tr/